



Article

Pellet-Based Extrusion Additive Manufacturing of Lightweight Parts Using Inflatable Hollow Extrudates

Md Ahsanul Habib, Rawan Elersawy and Mohammad Abu Hasan Khondoker *

Industrial Systems Engineering, Faculty of Engineering and Applied Science, University of Regina, Regina, SK S4S 0A2, Canada; mhy407@uregina.ca (M.A.H.); rre285@uregina.ca (R.E.)

* Correspondence: mohammad.khondoker@uregina.ca; Tel.: +1-306-585-4289

Abstract: Additive manufacturing (AM) has become a key element of Industry 4.0, particularly the extrusion AM (EAM) of thermoplastic materials, which is recognized as the most widely used technology. Fused Filament Fabrication (FFF), however, depends on expensive commercially available filaments, making pellet extruder-based EAM techniques more desirable. Large-format EAM systems could benefit from printing lightweight objects with reduced material use and lower power consumption by utilizing hollow rather than solid extrudates. In this study, a custom extruder head was designed and an EAM system capable of extruding inflatable hollow extrudates from a variety of materials was developed. By integrating a co-axial nozzle-needle system, a thermoplastic shell was extruded while creating a hollow core using pressurized nitrogen gas. This method allows for the production of objects with gradient part density and varied mechanical properties by controlling the inflation of the hollow extrudates. The effects of process parameters—such as extrusion temperature, extrusion speed, and gas pressure—were investigated—using poly-lactic acid (PLA) and styrene-ethylene-butylene-styrene (SEBS) pellets. The preliminary tests identified the optimal range of these parameters for consistent hollow extrudates. We then varied the parameters to determine their impact on the dimensions of the extrudates, supported by analyses of microscopic images taken with an optical microscope. Our findings reveal that pressure is the most influential factor affecting extrudate dimensions. In contrast, variations in temperature and extrusion speed had a relatively minor impact, whereas changes in pressure led to significant alterations in the extrudate's size and shape.



Academic Editor: Lawrence E. Murr

Received: 12 December 2024

Revised: 24 January 2025

Accepted: 26 January 2025

Published: 29 January 2025

Citation: Habib, M.A.; Elersawy, R.; Khondoker, M.A.H. Pellet-Based Extrusion Additive Manufacturing of Lightweight Parts Using Inflatable Hollow Extrudates. *J. Manuf. Mater. Process.* **2025**, *9*, 37. <https://doi.org/10.3390/jmmp9020037>

Copyright: © 2025 by the authors. Licensee MDPI, Basel, Switzerland. This article is an open access article distributed under the terms and conditions of the Creative Commons Attribution (CC BY) license (<https://creativecommons.org/licenses/by/4.0/>).

Keywords: additive manufacturing (AM); extrusion AM (EAM); Co-axial extrusion; inflatable extrudates; pellet extrusion; gradient part density

1. Introduction

Additive Manufacturing (AM), also known as 3D printing, has transformed the production environment into several sectors by enabling quick prototyping, customization, and the creation of complicated geometries that are not possible with traditional manufacturing processes [1–3]. The progression of additive manufacturing technologies has been characterized by ongoing innovation to surpass the constraints of conventional production processes. Historically, additive manufacturing has employed a variety of materials, such as polymers, metals, and ceramics, each possessing distinct characteristics that make them suited for certain uses. Thermoplastics have become prominent because of their flexibility, durability, and ease of usage [4]. They preferred materials in additive manufacturing because of their thermal properties, which enable them to be melted, molded, and solidified several times without substantial deterioration. This characteristic renders them well-suited

for methods like fused deposition modeling (FDM), in which the material is extruded via a heated nozzle to construct structures incrementally [5]. One of the key advantages of FDM technology is its flexibility, allowing users to modify the hot end and adjust the bed size to suit their specific printing needs [6–8].

The present trends in additive manufacturing are mostly centered around increasing the amount of output, attaining greater printing speeds through enhanced flow rates, and progressing toward large-scale additive manufacturing [9–11]. These trends create components that possess uniform structural integrity over their entire length. Pellet extruders are being used instead of filament extruders to attain higher speeds. Using pellet extruders in additive manufacturing offers advantages over traditional filament-based 3D printing. Pellet extruders use raw thermoplastic pellets, which are cheaper and more widely available, reducing material costs and allowing for a broader range of materials. This method also supports sustainable manufacturing by minimizing waste and energy use, making it ideal for scaling up industrial production with a smaller environmental footprint [12,13]. Nevertheless, new difficulties have occurred in the manufacturing process with the advancement of extruders. The manufacturing time is now limited by the cooling time of the material before the next layer can be printed, rather than the extrusion rate (kg/h) [14]. Moreover, larger bead sizes result in higher material usage, which might significantly affect the environmental effect of the printed objects. Hence, it is important to investigate alternate methodologies for large-scale 3D printing to mitigate its ecological repercussions. On the other hand, the inflatable hollow structures have filled the gap regarding the weight of the product and the time needed to process the production of aerospace and space exploration for deployable space habitats, communication balloons, lightweight fuel tanks, automotive and transport for airbags, adaptive aerodynamic components, and portable shelters for emergency responses. It may serve in architecture and buildings as a temporary shelter, formwork of concrete, event domes, and other related purposes [15]. Some examples of medical uses are rehabilitation, isolation units, and portable medical facilities, while for defense and military, this technology is employed for inflatable decoys, portable command centers, and rapid deployment shelters. Further applications include sport and recreation inflatable kayaks, stadium covers, playground structures, and much more. Applications involve life rafts, submerged research structures, oil spill barriers in marine, and consumer products comprising inflated furniture and packaging for protection and portable storage. It is also applied in robotics, which has soft robotic grippers, biomedical applications, and artificial muscles operated by compressed air [15]. These wide-ranging applications epitomize and signify how inflatable, hollow structures present State-of-the-Art solutions to various fields economically. However, the integration between pellet extrusion and inflatable hollow extrudates is limited in the literature.

This study aims to address several research questions related to optimizing 3D printing processes. First, explore whether hollow extrudates made of thermoplastics can be used to conserve material and expedite printing. Second, investigate the potential for adjusting the level of inflation during printing to customize the mechanical characteristics of components. Additionally, it will examine whether varying density levels can be achieved through 3D printing and assess the feasibility of using pellets instead of filaments to increase printing speed. These questions guide the inquiry into enhancing the efficiency and versatility of 3D printing technologies.

To fill this void, this research aims to design and develop a co-axial nozzle system for inflatable extrudates, integrate this custom nozzle system with a pellet extruder for 3D printing by modifying the existing printer, understand the effect of process parameters on the degree of inflation of the extrudates, and demonstrate proof-of-concept for 3D printing using inflated extrudates.

2. Materials and Methods

2.1. Material Selection

PLA and SEBS, two different polymers, were used in this experiment. Thermoplastic elastomer SEBS (styrene-ethylene-butylene-styrene) is renowned for its resilience to ozone and UV rays as well as its flexibility and durability [16]. Conversely, PLA, or polylactic acid, is a thermoplastic that degrades naturally and is environmentally friendly and easily processed. It comes from renewable resources [17,18]. The purpose of employing two distinct types of material is to test the versatility and effectiveness of the created approach to both materials and validate how each material would respond to different process settings and whether the outcomes would be the same for both kinds of polymers.

2.2. System Design

2.2.1. Extruder Head

A special hot-end extruder was designed and prepared from aluminum (Al) that met the requirements to extrude inflated thermoplastic rather than solid material. Because of the needle passing through the nozzle, the extrudate could be hollowed out by a regulated flow of nitrogen gas. A heater (120 V, 50 W) was mounted on the extruder to keep the temperature at the required level for this operation. Through the use of a soft PVC pipe, the needle was attached to an air pressure regulator, allowing it to adjust the gas pressure precisely and monitor the results at different gas pressure settings. The extruder head details are shown in Figure 1.

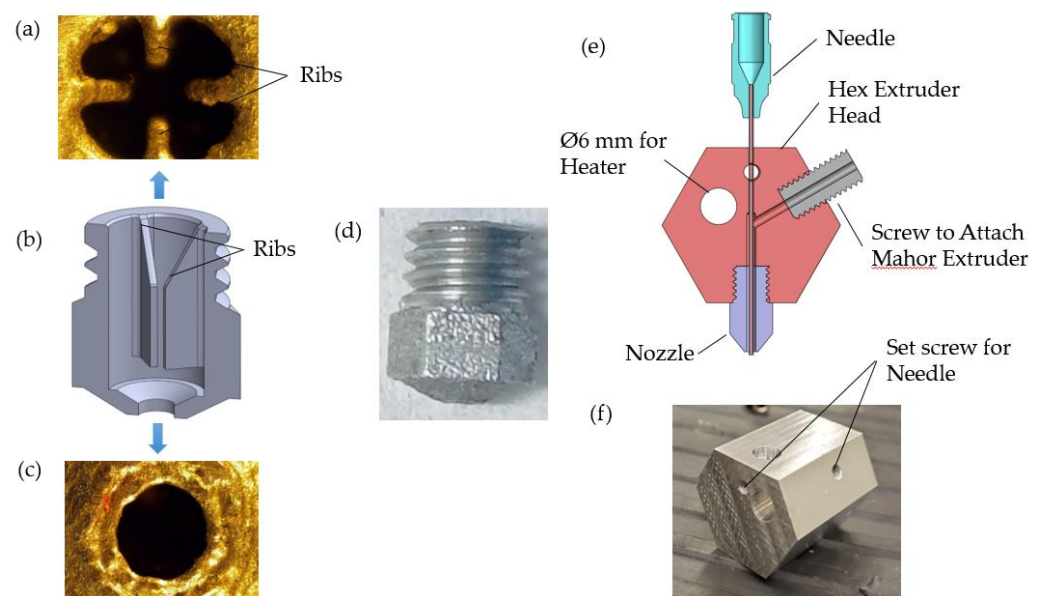


Figure 1. Extrusion nozzle: (a) Microscopic observation from top; (b) Cross-section of nozzles; (c) Microscopic observation from bottom; (d) Three-dimensional printed nozzle; (e) Transverse section view of Hot-end assembly; (f) Manufactured extruder head.

2.2.2. Nozzle Design

The nozzle and needle must remain concentric to guarantee exact control over the inflation and extrusion operations. Thus, selective laser melting (SLM) 3D printing technology was used to create a customized aluminum nozzle with four ribs to retain the needle at the center of the nozzle orifice.

A microscopic inspection of the samples was carried out using an OMAX optical microscope (OMAX Microscopes, <https://omaxmicroscope.com/>) to accurately assess surface characteristics and identify potential defects. A systematic inspection process was followed to ensure high-quality image analysis. To begin, the samples were thoroughly

cleaned to eliminate any dust, debris, or contaminants that might interfere with the inspection. Once cleaned, they were carefully placed on the microscope stage and positioned for optimal focus. The OMAX optical microscope, capable of magnifications up to $\times 100$ using visible light and lenses, was used to conduct basic surface inspections and detect any defects. External lighting was adjusted as needed to improve image clarity and contrast. Magnification and focus settings were fine-tuned to capture images at different depths within the sample layers, allowing for the detailed observation of features such as cracks, voids, surface roughness, and other imperfections. Multiple images were taken at varying magnifications by using ToupView and later superimposed to provide a comprehensive analysis of the sample's structure.

2.2.3. Hopper Design

The experiment required the alignment of the Mahor pellet extruder 30 degrees with the horizontal axis, as the needle, carrying nitrogen gas to be kept vertical, made the current hopper inappropriate for the setup (see Supplementary Figure S1). The hopper needs to stay upright to guarantee that the pellets flow naturally because of gravity. Therefore, the pellet extruder was coupled with a hopper that was printed in 3D in our lab.

2.2.4. Bracket Design

The extrusion mechanism of the used 3D printer (Crealty Ender-5 S1) was disassembled and a bracket system was created to securely attach the pellet extruder to the machine. This system was made up of two separate components: one was meant to keep the extruder firmly in place, while the other was meant to be attached to the 3D printer (Supplementary Figure S2). After that, screws were used to secure these two parts together, and the extruder was positioned at an exact 30-degree angle to the horizontal axis.

2.2.5. Mahor Pellet Extruder

The Mahor pellet extruder uses plastic pellets or granules as raw material, as opposed to conventional filament-based 3D printers that use plastic filament. Pellets are heated and melted in the extruder after being fed into it through a hopper at the start of the operation. After that, the melted material is pushed into the extruder nozzle, which follows a predetermined route and deposits the material layer by layer to create the desired item. An image of the Mahor pellet extruder is shown (Supplementary Figure S3).

2.3. Methodology

2.3.1. Process Flow

To produce inflatable hollow extrudates, a setup incorporating several components and modifications was designed to optimize the extrusion process, as shown in Figure 2. Initially, nitrogen gas was introduced into the system to inflate the extrudates. A cylinder was used to store nitrogen gas, with a digital air pressure sensor attached to the cylinder's outlet to precisely measure the gas flow. Pressure was controlled by a gas regulator. A flexible PVC pipe was used to connect the digital air pressure regulator to the needle and to transport the nitrogen gas from the cylinder to the nozzle orifice via the needle. Additionally, a temperature controller was used to maintain the required temperature at the hex extruder. The pellet was now fed into the Mahor through the hopper, melted inside, and was pushed to the hex extruder. The extrudate then extruded out the nozzle orifice, where it was inflated by the nitrogen gas carried by the needle.

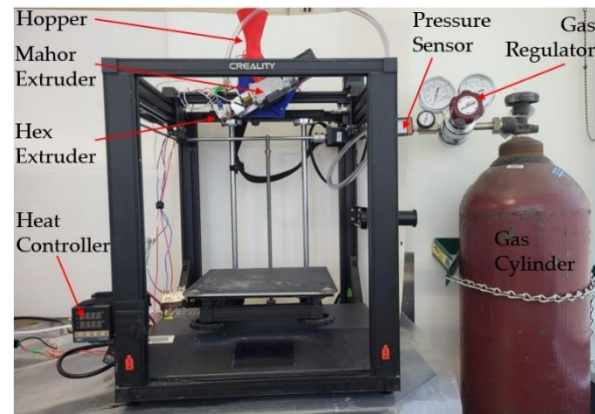


Figure 2. Experimental setup of the full extruder head mounted to the printer and the gas cylinder with the pressure sensor and regulator.

2.3.2. G-Code Generation

An innovative open-source software called FullControl GCode Designer (GNU GPL v3.0 open source license, <https://fullcontrolgcode.com/> (accessed on 10 April 2024)) was used to produce G-code for 3D printing. The best feature of this software is that every bit of the print path can be controlled. In addition, no CAD file or any slicing software is required. The software is an Excel-based interface. Within this interface, there is an option to add features. By selecting this option, any necessary feature can be called, and one can define its parameters and ultimately generate the required print path by clicking the “Generate Gcode” button. To preview the print path, a slicing software called Repetier-Host was utilized. If the preview appeared satisfactory, the G-code was saved onto a memory card, which was then inserted into the printer for the printing process.

2.3.3. Sample Generation

Initially, several simple components were printed using both PLA and SEBS materials, following the methodology described above. Initially, some spiral single-layer cylindrical parts were produced, as shown in Figure 3, and examined whether they remained hollow throughout the printing process by analyzing sample cross-sections.

Additionally, colored water was injected with a needle from one end of the cylindrical sample and observed whether the colored water successfully reached the opposite end, which it did. Following that, cylindrical samples with multiple layers in both vertical and horizontal directions were printed.

One of the major objectives of this experiment was to produce parts with gradient part density with tailored mechanical properties throughout the part by controlling the rate of inflation of the hollow extrudates. To print the gradient density part, we came up with a design with two different portions, with one portion looking like a C-shape printed with solid layers (no inflation) with 1.0 mm of height. After printing 2 layers in this region, we started printing the semicircular region with inflation, which had a height of 2.0 mm, and then repeated the printing of the no-inflation zone, as shown in Figure 3.

Using this technique, four inflated layers in the semicircular half and a total of eight solid layers in the C-shaped half were printed. The fundamental goal of the experiment was effectively achieved by this method, which produced an item with two unique densities in its respective sections. Nitrogen gas was passed, and the inflation was manually regulated.

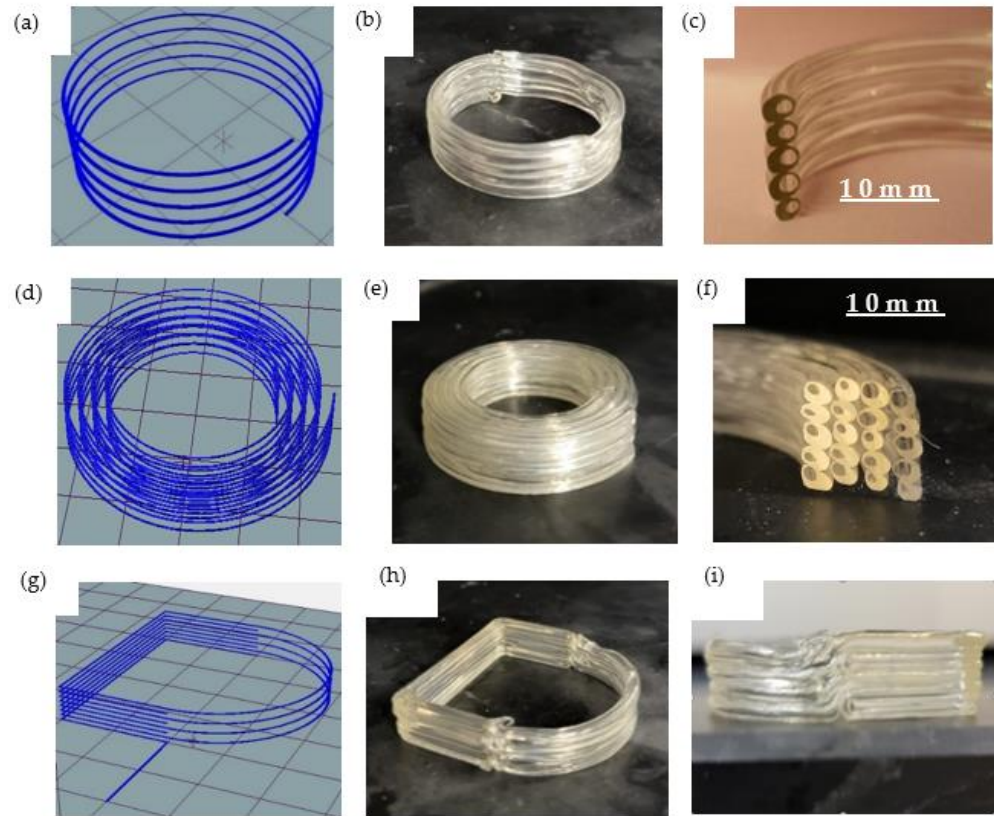


Figure 3. Spiral Cylindrical Printed Part: (a) Print Path Preview; (b) Printed Part; (c) Cross-section. Multi-layer cylindrical part: (d) Print path preview; (e) Printed part; (f) Cross-section. Part with gradient density: (g) Print path; (h) Printed part; (i) Front view.

3. Analytical Modeling

An analytical model was developed to analyze the behavior of the polymer inside the nozzle. The system consists of two concentric cylinders, the needle and the nozzle, where the polymer flows through the annular gap between these two stationary, vertically aligned cylinders. This type of flow is known as an annular flow [19]. The outer radius of the needle is denoted as R_i and the inner radius of the nozzle as R_o . A pressure difference ΔP drives the polymer, which has a certain viscosity μ , to flow downward. We aimed to determine the velocity profile within the annular space V and calculate the total volumetric flow rate Q using a cylindrical coordinate system.

To derive the velocity equation, the continuity equation and Navier–Stokes equation for the z -component of velocity in cylindrical coordinates was used. With the help of a few assumptions and boundary conditions following velocity, equation was derived. The whole derivation is shown in Supplementary Section S4.

$$V_z = \frac{1}{4\mu} \left(-\frac{\partial P}{\partial z} + \rho g \right) \left[R_i^2 - r^2 + \frac{(R_o^2 - R_i^2)}{\ln \frac{R_o}{R_i}} \ln \frac{r}{R_i} \right]$$

By integrating the velocity profile $V_z(r)$ over the cross-sectional area A of the annulus, we obtained the equation for the volumetric flow rate Q .

$$Q = \int V_z(r) dA$$

In cylindrical coordinates, the differential area element dA is $2\pi r dr$.

$$Q = \int_{R_i}^{R_o} V_z(r) 2\pi r dr$$

$$Q = \frac{\pi(R_o^2 - R_i^2)}{8\mu} \left(-\frac{\partial P}{\partial z} + \rho g \right) \left(R_o^2 + R_i^2 - \frac{(R_o^2 - R_i^2)}{\ln\left(\frac{R_o}{R_i}\right)} \right)$$

The driving force of the flow is explained by the expression $\left(-\frac{\partial P}{\partial z} + \rho g\right)$. It combines the forces of gravity and the pressure gradient, which push and pull the fluid, respectively. Because of the annular shape, the velocity profile fluctuates as a mixture of parabolic and logarithmic components and is not constant across the radial direction as appears in Figure 4a. The pressure gradient, gravity, viscosity, and annulus geometry all affect the flow rate.

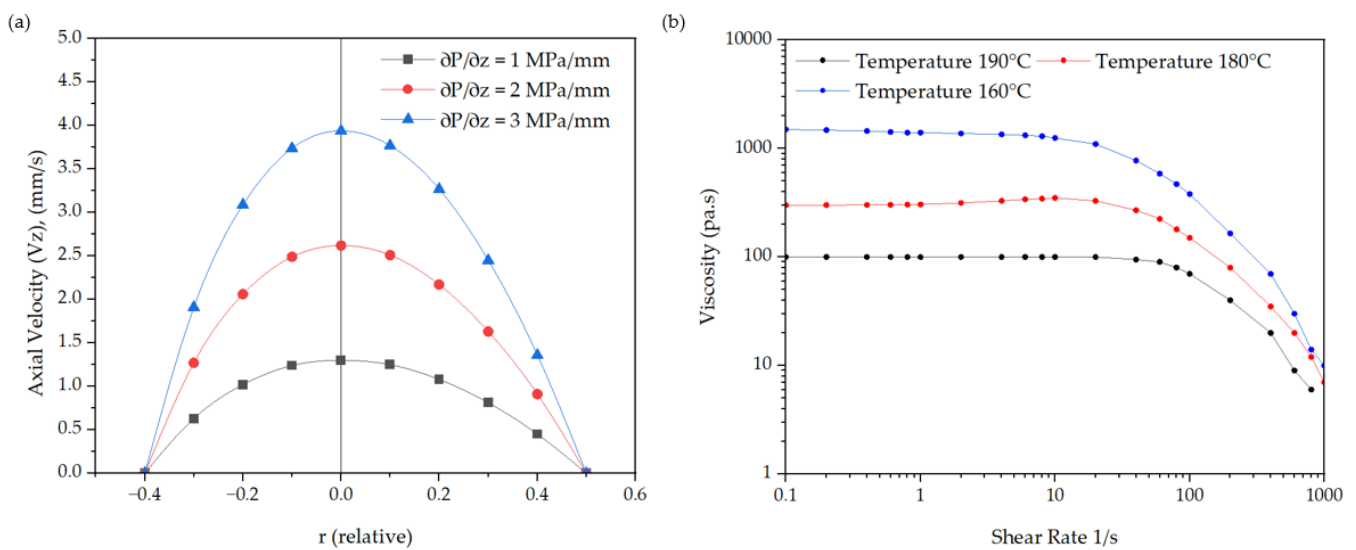


Figure 4. (a) Velocity profile for different pressure gradients; (b) Viscosity as a function of temperature and shear rate for Amorphous PLA.

Few assumptions were made for computation purposes because measuring them was impossible. Since pressure could not be found directly, three different pressure gradients were looked at, namely $\frac{\partial P}{\partial z} = 1$ MPa/mm, 2 MPa/mm, and 3 MPa/mm. Figure 4b was used to compute the PLA’s viscosity (μ). A viscosity of 70 Pa.s. was assumed, and the experiment was carried out at two different temperatures: 205°C and 220°C .

For three distinct pressure gradients, the velocity at the nozzle’s cylindrical section was computed. The cylindrical part of the nozzle had an inner diameter of 2.5 mm and an outer diameter of 0.70 mm. The velocity between the nozzle’s inner diameter and needle’s outer diameter was computed and recorded at each pressure and a distinct radial position, as shown in Table 1. These numbers were later put onto a graph (see Figure 5a).

Table 1. Velocity in the cylindrical zone for different assumed pressure gradient.

r (mm)	r (Relative)	V_z (mm/s)		
		$\frac{\partial P}{\partial z} = 1$ MPa/mm	$\frac{\partial P}{\partial z} = 2$ MPa/mm	$\frac{\partial P}{\partial z}$
0.35	−0.4	0.00	0.00	0.00
0.45	−0.3	0.63	1.27	1.91
0.55	−0.2	1.02	2.06	3.09

Table 1. Cont.

r (mm)	r (Relative)	V _z (mm/s)		
		$\frac{\partial P}{\partial z} = 1 \text{ MPa/mm}$	$\frac{\partial P}{\partial z} = 2 \text{ MPa/mm}$	$\frac{\partial P}{\partial z}$
0.65	-0.1	1.24	2.49	3.74
0.75	0	1.30	2.62	3.94
0.85	0.1	1.25	2.51	3.77
0.95	0.2	1.08	2.17	3.27
1.05	0.3	0.81	1.63	2.45
1.15	0.4	0.45	0.91	1.36
1.25	0.5	0.00	0.00	0.00

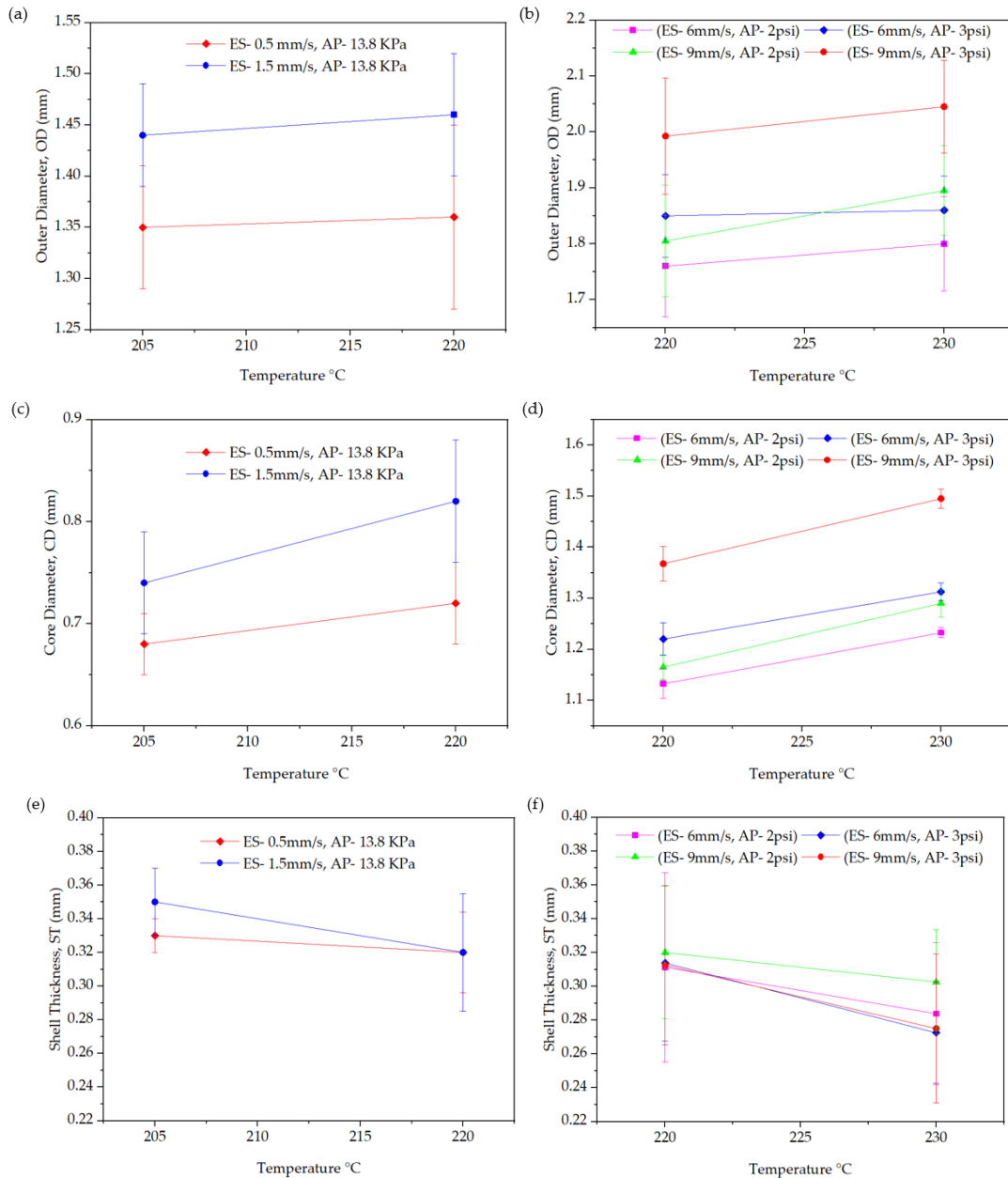


Figure 5. (a) Outer diameter of PLA extrudates as a function of temperature; (b) Outer diameter of SEBS extrudates as a function of temperature; (c) Core diameter of PLA extrudates as a function of temperature; (d) Core diameter of SEBS extrudates as a function of temperature; (e) Shell thickness of PLA extrudates as a function of temperature; (f) Shell thickness of SEBS extrudates as a function of temperature.

4. Results and Discussion

4.1. Process Parameters

Extrusion temperature, extrusion speed, and gas pressure were three process parameters in our experiment. Two distinct temperatures were used for our experiment, namely 205 °C and 220 °C for PLA and 220 °C and 230 °C for SEBS. The lower limit represents the minimum threshold required for sufficient material flow through the nozzle, while the upper limit is just below the degradation point of the plastic, beyond which bubble bursting and non-uniform extrusion occurs. The extrusion speed and gas pressure for each temperature, while maintaining a fixed nozzle diameter, were changed to find the maximum and lowest values of the extrudates for each parameter (extrusion speed and gas pressure). The minimum pressure was selected, as values below this could not be accurately detected, while the maximum was limited to prevent poor extrusion quality and bubble bursting. While the extrusion speed was carefully chosen to ensure optimal inflation; lower speeds resulted in inadequate extrusion, while higher speeds exceeded the motor’s capacity. Five sets of samples were made for every combination of temperature, extrusion speed, and gas pressure. The average outer diameter, core diameter, and shell thickness of each sample were measured by microscopically examining their tiny cross-sections. The data for PLA and SEBS are recorded under various process settings in Table 2 and Table 3, respectively.

Table 2. Data Collection for Different Extrusion Parameters (PLA).

Nozzle Diameter	Extrusion Temperature (°C)	Extrusion Speed (mm/s)	Gas Pressure (KPa)	Average Outer Diameter (D) (mm)	Average Core Diameter (d) (mm)	Average Shell Thickness (t) (mm)
1.5	220	0.5	13.8	1.36 ± 0.05	0.72 ± 0.06	0.32 ± 0.055
			17.2	1.39 ± 0.07	0.77 ± 0.07	0.31 ± 0.07
1.5	220	1.5	13.8	1.46 ± 0.06	0.82 ± 0.02	0.32 ± 0.04
			24.1	1.64 ± 0.08	1.02 ± 0.02	0.31 ± 0.05
1.5	220	2.5	13.8	1.55 ± 0.07	0.85 ± 0.04	0.35 ± 0.055
			27.6	1.79 ± 0.10	1.09 ± 0.03	0.35 ± 0.065
1.5	220	3	13.8	1.60 ± 0.07	0.87 ± 0.04	0.37 ± 0.055
			27.6	1.95 ± 0.02	1.23 ± 0.02	0.36 ± 0.02
1.5	205	0.5	13.8	1.35 ± 0.06	0.68 ± 0.03	0.33 ± 0.045
			27.6	1.56 ± 0.04	0.93 ± 0.07	0.31 ± 0.055
1.5	205	1.5	13.8	1.44 ± 0.09	0.74 ± 0.03	0.35 ± 0.06
			27.6	1.59 ± 0.07	0.93 ± 0.04	0.33 ± 0.055

Table 3. Data Collection for different Extrusion Parameters (SEBS).

Nozzle Diameter	Extrusion Temperature (°C)	Extrusion Speed (mm/s)	Gas Pressure (KPa)	Average Outer Diameter (D) (mm)	Average Core Diameter (d) (mm)	Average Shell Thickness (t) (mm)
1.5	220	3	13.8	1.70	1.11	0.30
			20.7	1.75	1.16	0.30
1.5	220	6	13.8	1.76	1.13	0.31
			20.7	1.85	1.22	0.31
1.5	220	9	13.8	1.81	1.17	0.32
			20.7	1.99	1.37	0.31
1.5	230	3	13.8	1.74	1.20	0.27
			20.7			
1.5	230	6	13.8	1.80	1.23	0.28
			20.7	1.86	1.31	0.27
1.5	230	9	13.8	1.90	1.29	0.30
			20.7	2.05	1.50	0.28

4.2. Effect of Temperature

The experiment demonstrated that temperature had a significant impact on the dimensions of the extrudates. As the extrusion temperature increased, noticeable trends emerged in the dimensional characteristics of the extrudates for both PLA and SEBS materials. For PLA, raising the temperature from 205 °C to 220 °C led to a significant expansion in both the outer and inner diameters of the extrudates, while the shell thickness decreased. This can be attributed to the lower viscosity at higher temperatures [20], which allows the molten PLA to flow more easily and expand more under the influence of nitrogen gas pressure. With reduced resistance to deformation, the applied pressure causes greater radial expansion, resulting in larger diameters. At the same time, the decreased viscosity enables greater stretching of the extruded walls, leading to a thinner shell.

A similar trend was observed in SEBS extrudates, where increasing the extrusion temperature from 220 °C to 230 °C resulted in an expansion of both the outer and core diameters, along with a reduction in shell thickness. Although SEBS, as a thermoplastic elastomer, has different rheological properties compared to PLA, it also experiences a drop in viscosity at higher temperatures. This reduction allows the material to be displaced more easily under pressure, contributing to the observed expansion in diameter. The thinning of the shell suggests that at elevated temperatures, the material undergoes increased stretching and thinning during inflation, further influenced by the elastic nature of SEBS. This relationship was consistent across two different conditions for PLA and four different conditions for SEBS, indicating that temperature control is crucial for achieving the desired dimensions and mechanical properties in the final extruded product. The results are supported by similar findings found in literature [20]. Figure 5 shows the effect of temperature on extrudates dimensions for both PLA and SEBS.

4.3. Effect of Gas Pressure

Gas pressure was another important factor in defining the extrudates' size. Increasing gas pressure had a significant impact on the dimensional characteristics of the extrudates, causing both the core and outer diameters to expand while simultaneously reducing the shell thickness, assuming all other factors remained constant. This effect can be explained by the greater force exerted by the nitrogen gas on the molten thermoplastic, which enhances the inflation of the extrudate [21]. As the pressure increases, more gas is introduced into the molten PLA, leading to a more pronounced expansion that results in larger core and outer diameters. However, this expansion also stretches the extrudate walls, causing the shell thickness to decrease as the material is redistributed over a larger volume.

A similar trend was observed with SEBS, where increasing the gas pressure from 13.8 KPa to 20.7 KPa across different process conditions produced the same effects, that is, an increase in both outer and core diameters, accompanied by a thinner shell. The way SEBS responds to higher pressure closely mirrors that of PLA, suggesting that the inflation dynamics are primarily influenced by the interaction between internal gas pressure and the material's viscoelastic properties as reported in literature [21]. For both PLA and SEBS materials, Figure 6 illustrates how variations in gas pressure affect the materials' outer diameter (OD), core diameter (CD), and shell thickness (ST), while maintaining constant values for the other parameters.

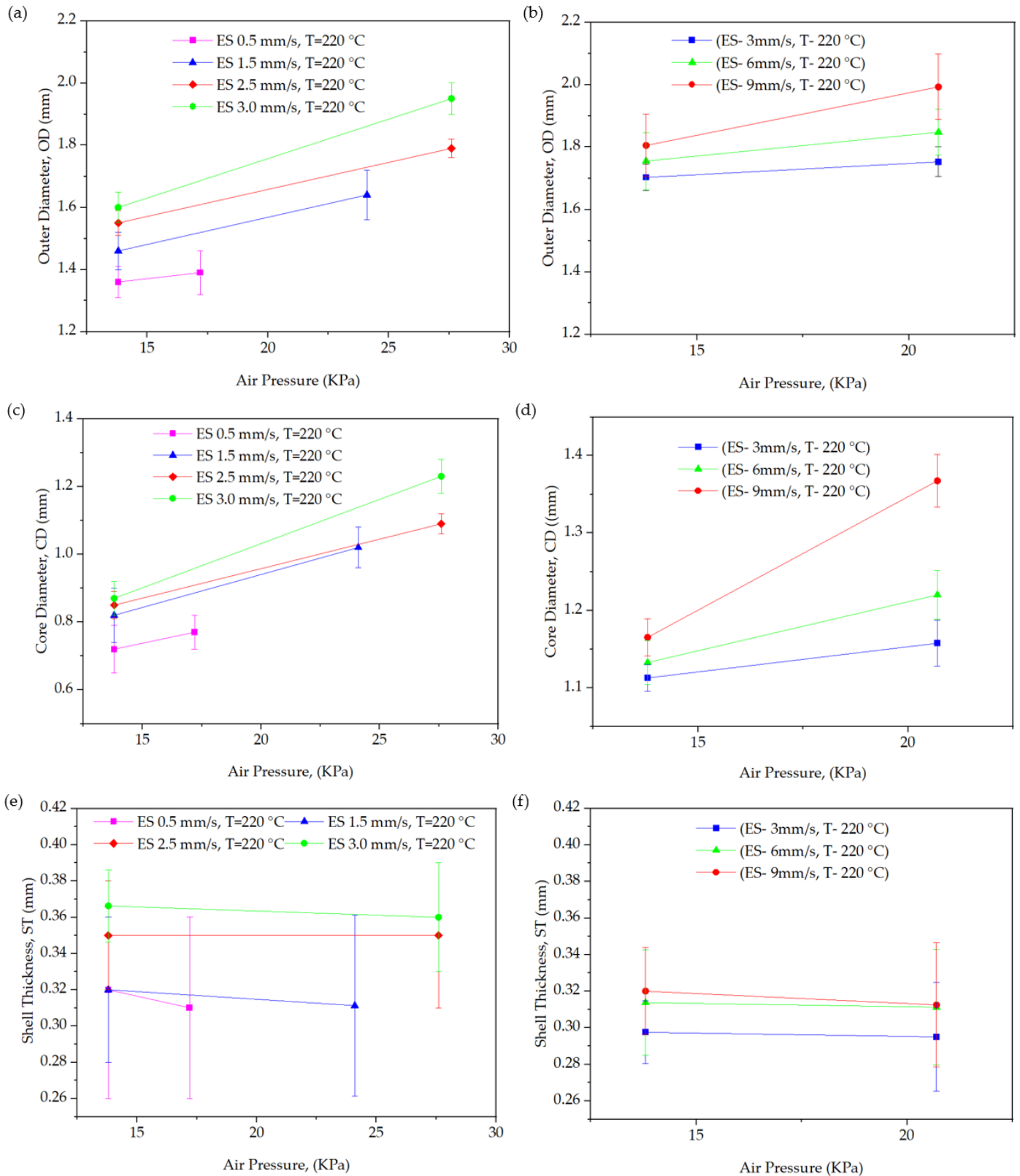


Figure 6. (a) Effect of gas pressure on PLA extrudates' outer diameter; (b) Effect of gas pressure on SEBS extrudates' outer diameter; (c) Effect of gas pressure on PLA extrudates' core diameter; (d) Effect of gas pressure on SEBS extrudates' core diameter; (e) Effect of gas pressure on PLA extrudates' shell thickness; (f) Effect of gas pressure on SEBS extrudates' shell thickness.

4.4. Effect of Extrusion Speed

The diameters of the extrudates were significantly influenced by the extrusion speed as well. Increasing the extrusion speed while keeping the temperature and gas pressure constant led to a proportional increase in the outer diameter, core diameter, and shell thickness of the extrudates. This effect can be attributed to the higher volumetric flow rate, which introduces more material into the system, allowing for greater expansion under the same inflation conditions. As the extrusion speed increases, the additional material provides more mass for the nitrogen gas to act upon, resulting in the formation of larger and thicker extrudates [22]. The higher flow rate allows the thermoplastic to expand further before solidifying, contributing to an overall increase in dimensional attributes.

This trend was consistently observed in both PLA and SEBS materials across different temperature settings. For PLA, experiments conducted at 205 °C and 220 °C showed similar responses to changes in extrusion speed, while SEBS exhibited comparable behavior at 220 °C and 230 °C. These findings indicate that the expansion dynamics are primarily driven by the relationship between extrusion speed and material flow, with both materials responding predictably to variations in process parameters, as depicted in literature [22]. The impact of extrusion speed on extrudate dimensions for PLA and SEBS, respectively, is depicted in Figure 7.

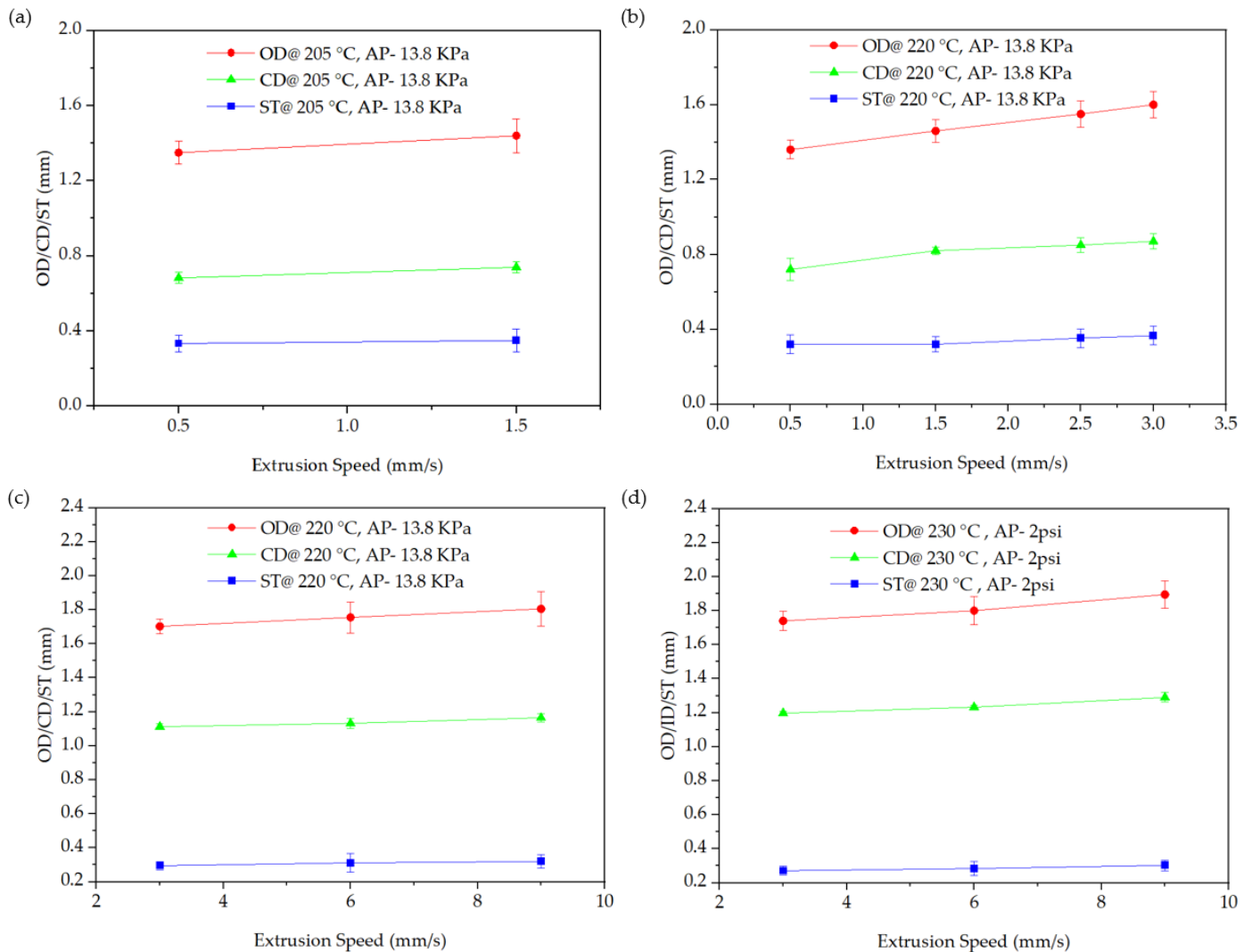


Figure 7. Effect of extrusion speed over OD/ID/ST: (a) at 205 °C with PLA, and (b) at 220 °C with PLA; effect of extrusion speed over OD/CD/ST: (c) at 220 °C with SEBS, and (d) at 230 °C with SEBS.

4.5. Morphological Observation

Microscopic images were collected under varied settings for both PLA and SEBS, as indicated below. In Figures 8 and 9, we have shown the effect of three different process parameters over the dimension of extrudate. The notation ‘1.5_205_0.5_13.8’ means that the sample was produced using a 1.5 mm diameter nozzle, at a temperature of 205 °C, with an extrusion speed of 0.5 mm/s, and a gas pressure of 13.8 KPa.

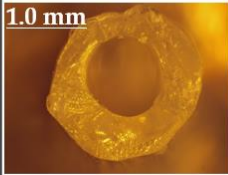
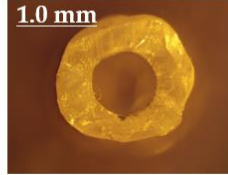
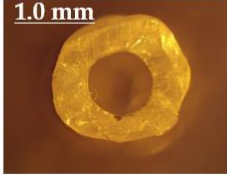
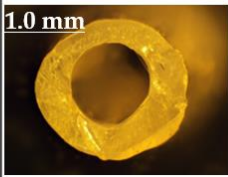
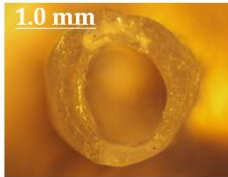
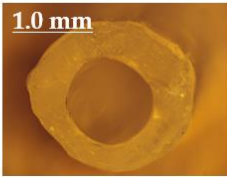
Effect of Temperature		Effect of Air Pressure		Effect of Extrusion Speed	
1.5_T_1.5_13.8		1.5_205_0.5_AP		1.5_220_ES_13.8	
205 °C		13.8 KPa		0.5 mm/s	
220 °C		27.6 KPa		3.0 mm/s	

Figure 8. Microscopic observation of PLA Extrudates cross-sections.

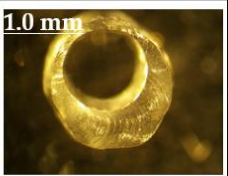
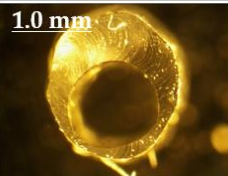
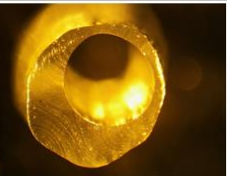
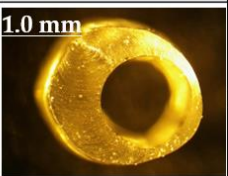
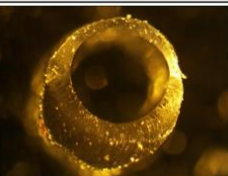
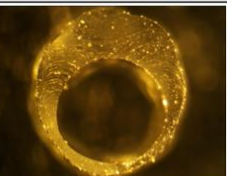
Effect of Temperature		Effect of Air Pressure		Effect of Extrusion Speed	
1.5_T_3.0_13.8		1.5_220_6.0_AP		1.5_220_ES_20.7	
220 °C		13.8 KPa		3.0 mm/s	
230 °C		20.7 KPa		9.0 mm/s	

Figure 9. Microscopic observation of cross-sections of SEBS extrudates.

5. Conclusions

The development of additive manufacturing with inflatable thermoplastics faced challenges in maintaining temperature, air pressure, and material flow consistency. Temperature fluctuations affected thermoplastic viscosity and extrudate quality, while air pressure variations led to inconsistencies in wall thickness and structure. Material flow issues caused variability in part mass, twisting, and eccentric hollow structures, affecting precision. Manual adjustments for nitrogen gas pressure introduced further inconsistencies, highlighting the need for automated control. Nozzle clogging and wear over time also impacted quality. Despite these challenges, valuable insights were gained to improve process control, automation, and material consistency for enhanced reliability and efficiency. The successful establishment of a methodology for producing inflatable extrudates using a pellet extruder provides a solid foundation for further research. However, improvements in process accuracy and efficiency are needed. Upgrading equipment such as pressure regulators and temperature controllers will enhance stability and precision. Comprehensive mechanical testing, including tensile and impact assessments, is essential to evaluate properties and

applications. Comparative studies on thermal and acoustic insulation will demonstrate the advantages of hollow extrudates over solid materials. Optimizing adhesion and layer bonding, scaling up with larger nozzles, and exploring real-world applications in the aerospace, automotive, and construction sectors will support commercialization.

Additive manufacturing has advanced significantly since the 1980s, but challenges persist in creating complex structures with varying densities. This study introduced a novel method to control the expansion of thermoplastic extrudates by optimizing key parameters such as extrusion temperature, gas pressure, and extrusion speed, using PLA and SEBS. Results showed that increasing temperature and air pressure led to larger outer and core diameters with reduced shell thickness, while higher extrusion speeds increased all dimensions. Gas pressure had the most significant influence. A mathematical model provided insights into polymer behavior within the nozzle. Inflated spiral cylindrical and multi-layer cylindrical samples were successfully produced, enabling gradient density structures by varying inflation rates. Existing studies on hollow extrudates primarily focus on structural integrity and mechanical properties, which differ from this study's goal of optimizing process parameters. The findings highlight the potential of inflatable extrudates for enhanced thermal insulation in applications such as packaging, construction, and protective enclosures, while controlled density gradients offer opportunities for energy absorption in impact-resistant components and cushioning materials.

In conclusion, this research establishes a foundation for controlled inflation of thermoplastic extrudates, offering promising opportunities for lightweight, durable, and customizable structures in various industries.

Supplementary Materials: The following supporting information can be downloaded at: <https://www.mdpi.com/article/10.3390/jmmp9020037/s1>. Section S1: The three-dimensional design of the used Hopper. Section S2: The printed Bracket using blue PLA. Section S3: Mahor Pellet Extruder. Section S4: Derivation of the Analytical Model. Figure S1: 3D CAD design of Hopper. Figure S2: Manufactured Bracket. Figure S3: Mahor Pellet Extruder.

Author Contributions: Conceptualization, M.A.H. and M.A.H.K.; Methodology, M.A.H. and R.E.; Validation, M.A.H.; Formal Analysis, M.A.H.; Investigation, M.A.H.; Resources, M.A.H.K.; Data Curation, R.E.; Writing—Original Draft Preparation, M.A.H.; Writing—Review & Editing, M.A.H., R.E. and M.A.H.K.; Visualization, M.A.H. and R.E.; Supervision, M.A.H.K.; Project Administration, M.A.H.K.; Funding Acquisition, M.A.H.K. All authors have read and agreed to the published version of the manuscript.

Funding: The work was funded by the Natural Sciences and Engineering Research Council of Canada, and the Government of Saskatchewan, Regina, SK, Canada.

Data Availability Statement: All data underlying the results are available as part of the article and Supplementary Materials, no additional sources are required.

Conflicts of Interest: The authors declare no conflicts of interest.

References

1. Gao, W.; Zhang, Y.; Ramanujan, D.; Ramani, K.; Chen, Y.; Williams, C.B.; Wang, C.C.L.; Shin, Y.C.; Zhang, S.; Zavattieri, P.D. The status, challenges, and future of additive manufacturing in engineering. *Comput.-Aided Des.* **2015**, *69*, 65–89. [[CrossRef](#)]
2. Gibson, I.; Rosen, D.W.; Stucker, B. *Additive Manufacturing Technologies*; Springer: New York, NY, USA, 2010.
3. Ngo, T.D.; Kashani, A.; Imbalzano, G.; Nguyen, K.T., Q.; Hui, D. Additive manufacturing (3D printing): A review of materials, methods, applications, and challenges. *Compos. Part B Eng.* **2018**, *143*, 172–196. [[CrossRef](#)]
4. Spatial. What Is Additive Manufacturing? (Types, Materials, and What to Know). 2023. Spatial Blog. 27 February. Available online: <https://blog.spatial.com/what-is-additive-manufacturing> (accessed on 5 May 2024).
5. Shanmugam, V.; Babu, K.; Kannan, G.; Mensah, R.A.; Samantaray, S.K.; Das, O. The thermal properties of FDM printed polymeric materials: A review. *Polym. Degrad. Stab.* **2024**, *228*, 110902. [[CrossRef](#)]

6. Daramwar, V.; Kadam, S. Design and development of multi-material extrusion in FDM 3D printers. *Int. J. Adv. Res. Sci. Eng. Technol.* **2020**. Available online: <https://www.irjet.net/archives/V7/i3/IRJET-V7I3731.pdf> (accessed on 5 May 2024).
7. Ali, M.H.; Kurokawa, S.; Shehab, E.; Nizam, I. Development of a large-scale multi-extrusion FDM printer, and its challenges. *Int. J. Eng. Technol.* **2023**, *19*, 123–134. Available online: <https://www.sciencedirect.com/science/article/pii/S2588840422000701> (accessed on 6 May 2024). [[CrossRef](#)]
8. Shaik, Y.P.; Schuster, J.; Shaik, A. A scientific review on various pellet extruders used in 3D printing FDM processes. *Open Access Libr. J.* **2021**, *8*, 1–14. Available online: <https://www.scirp.org/journal/paperinformation?paperid=110955> (accessed on 6 May 2024). [[CrossRef](#)]
9. Huang, Y.; Leu, M.C.; Mazumder, J.; Donmez, A. Additive Manufacturing: Current State, Future Potential, Gaps and Needs, and Recommendations. *J. Manuf. Sci. Eng.* **2014**, *137*, 014001. [[CrossRef](#)]
10. Campbell, I.; Bourell, D.; Gibson, I. Additive manufacturing: Rapid prototyping comes of age. *Rapid Prototyp. J.* **2012**, *18*, 255–258. Available online: https://www.researchgate.net/publication/263593130_Additive_manufacturing_Rapid_prototyping_comes_of_age (accessed on 10 May 2024). [[CrossRef](#)]
11. Altıparmak, S.C.; Yardley, V.A.; Shi, Z.; Lin, J. Extrusion-based additive manufacturing technologies: State of the art and future perspectives. *J. Manuf. Process.* **2022**, *75*, 209–231. Available online: <https://www.sciencedirect.com/science/article/pii/S1526612522006521> (accessed on 10 May 2024). [[CrossRef](#)]
12. Duhduh, A.; Noor, H.; Kundu, A.; Coulter, J. Advanced additive manufacturing of functionally gradient multi-material polymer components with single extrusion head: Melt rheology analysis. In Proceedings of the ANTEC. SPE TECHNICAL CONFERENCE AND EXHIBITION, 2019. Available online: <https://www.researchgate.net/publication/339585944> (accessed on 16 July 2024).
13. Murr, L.E.; Gaytan, S.M.; Medina, F.; Lopez, H.; Martinez, E.; Machado, B.I.; Hernandez, D.H.; Martinez, L.; Lopez, M.I.; Wicker, R.B.; et al. Next-generation biomedical implants using additive manufacturing of complex, cellular and functional mesh arrays. *Philos. Trans. R. Soc. A Math. Phys. Eng. Sci.* **2010**, *368*, 1999–2032. [[CrossRef](#)] [[PubMed](#)]
14. Go, J.; Schiffres, S.N.; Stevens, A.G.; Hart, A.J. Rate limits of additive manufacturing by fused filament fabrication and guidelines for high-throughput system design. *Addit. Manuf.* **2017**, *16*, 1–11. [[CrossRef](#)]
15. Morin, S.A.; Kwok, S.W.; Lessing, J.; Ting, J.; Shepherd, R.F.; Stokes, A.A.; Whitesides, G.M. Elastomeric tiles for the fabrication of inflatable structures. *Adv. Funct. Mater.* **2014**, *24*, 5541–5549. [[CrossRef](#)]
16. Kuraray. Styrene-Ethylene-Butylene-Styrene Thermoplastic Elastomer (SEBS). Kuraray Elastomer. Available online: <https://www.elastomer.kuraray.com/us/blog/sebs/> (accessed on 20 June 2024).
17. Wevolver. A Comprehensive Guide to PLA Melting Point and How It Influences 3D Printing. Wevolver. Available online: <https://www.wevolver.com/article/a-comprehensive-guide-to-pla-melting-point-and-how-it-influences-3d-printing> (accessed on 12 June 2024).
18. 3D Systems. Introduction to the Most Common Materials Used for 3D Printing. 3D Systems. Available online: <https://www.3ds.com/make/solutions/blog/most-common-materials-3d-printing> (accessed on 5 May 2024).
19. Wilkes, J.O. *Fluid Mechanics for Chemical Engineers with Microfluidics and CFD*, 2nd ed.; O'Reilly Online Learning; Available online: <https://www.oreilly.com/library/view/fluid-mechanics-for/9780132442329/ch06.html> (accessed on 23 June 2024).
20. Wang, J.; Porter, R.S. On the viscosity-temperature behavior of polymer melts. *Rheol. Acta* **1995**, *34*, 496–503. [[CrossRef](#)]
21. Powell, P.C.; Ingen Housz, A.J. *Engineering with Polymers*, 2nd ed.; CRC Press, 2023; Available online: <https://books.google.lu/books?id=JKlg2OhrHIMC&printsec=frontcover&hl=de#v=onepage&q&f=false> (accessed on 23 June 2024).
22. Duty, C.; Ajinjeru, C.; Kishore, V.; Compton, B.; Hmeidat, N.; Chen, X.; Liu, P.; Hassen, A.A.; Lindahl, J.; Kunc, V. What makes a material printable? A viscoelastic model for extrusion-based 3D printing of polymers. *J. Manuf. Process.* **2018**, *35*, 526–537. [[CrossRef](#)]

Disclaimer/Publisher's Note: The statements, opinions and data contained in all publications are solely those of the individual author(s) and contributor(s) and not of MDPI and/or the editor(s). MDPI and/or the editor(s) disclaim responsibility for any injury to people or property resulting from any ideas, methods, instructions or products referred to in the content.